Electronic structure study of triangular lattices in $FeGa_2S_4$, $Fe_2Ga_2S_5$, and $NiGa_2S_4$: Photoemission spectroscopy and Hartree-Fock calculations

K. Takubo,[1] T. Mizokawa,[1] Y. Nambu,[2] and S. Nakatsuji[2]
[1]*Department of Physics and Department of Complexity Science and Engineering, University of Tokyo, Chiba 277-8561, Japan*
[2]*Institute for Solid State Physics, University of Tokyo, Chiba 277-8581, Japan*
(Received 14 October 2008; revised manuscript received 28 December 2008; published 20 April 2009)

We have studied the electronic structure of the Fe and Ni triangular lattices in $FeGa_2S_4$, $Fe_2Ga_2S_5$, and $NiGa_2S_4$ using photoemission spectroscopy measurements, configuration-interaction calculations on FeS_6 and NiS_6 cluster models, and unrestricted Hartree-Fock calculations on FeS_2 and NiS_2 triangular lattices. The cluster-model analysis of the Fe $2p$ core-level spectra shows that the S $3p$ to Fe $3d$ charge-transfer energy Δ is $\sim$2.5 eV in $FeGa_2S_4$ and $Fe_2Ga_2S_5$, in contrast to the small Δ (~ -1 eV) found in $NiGa_2S_4$. The relationship between the Δ value and the superexchange pathway has been examined using the unrestricted Hartree-Fock calculations. In $FeGa_2S_4$ and $Fe_2Ga_2S_5$, the superexchange interaction between the nearest-neighbor sites is dominant while that between the third-nearest-neighbor sites is enhanced in $NiGa_2S_4$.

DOI: 10.1103/PhysRevB.79.134422 PACS number(s): 75.30.Et, 79.60.−i, 75.50.−y

I. INTRODUCTION

The triangular lattice is the simplest form of geometrically frustrated lattice in two dimensions, and has been extensively studied to search for spin-disordered states.[1–3] The newly discovered $NiGa_2S_4$ has the Ni^{2+} ($S=1$) triangular lattice layer without orbital degeneracy and found to have a spin-disordered ground state using neutron-diffraction experiment and nuclear quadrupole resonance experiment.[4,5] The neutron result also indicates that the spin-spin correlation between the third-nearest neighbors is much stronger than that between the first- and second-nearest neighbors, indicating that the conventional triangular lattice model with the nearest-neighbor superexchange coupling is not enough to describe $NiGa_2S_4$. $FeGa_2S_4$, which is an isostructural compound of $NiGa_2S_4$, also forms a frozen spin-disordered state within the Fe^{2+} triangular lattice,[6] although the Fe^{2+} state has spin $S=2$ twice larger than $S=1$ of $NiGa_2S_4$ and has partially occupied t_{2g} subshell that is fully occupied in $NiGa_2S_4$ (see Fig. 1). The spins of both compounds basically obey two-dimensional antiferromagnetic Heisenberg-type interactions and have no long-range order even at the lowest temperature. The magnetic part of the specific heats at low temperature has T^2 dependence and does not depend on applied magnetic field, indicating a peculiar short-range noncollinear order with two-dimensional gapless and linearly dispersive excitations on the frustrated lattice. While various theoretical proposals have been made for the two-dimensional coherent behavior of the specific heats,[8–13] the microscopic origin of the magnetic interactions in $FeGa_2S_4$ has not been clarified yet. In contrast, $Fe_2Ga_2S_5$ is a bilayered system of the Fe^{2+} triangular lattice and exhibits an antiferromagnetic order at $T_N \sim 113$ K. It is expected that the three-dimensional long-range order in $Fe_2Ga_2S_5$ is derived from the strong Fe-S-Fe interlayer bonds.

In order to understand the origin of the unusual magnetic properties of $FeGa_2S_4$, $Fe_2Ga_2S_5$, and $NiGa_2S_4$, it is highly important to clarify their underlying electronic structures. Previous study of photoemission and subsequent model calculation on $NiGa_2S_4$ has revealed that the ground state of $NiGa_2S_4$ has the d^9L character (L is a S $3p$ hole) and that the strong S $3p$ hole character of the ground state provides the enhanced superexchange interaction between the third-nearest-neighbor sites.[7] $NiGa_2S_4$ is a unique spin-disordered system in that the negative charge-transfer energy allows relatively long superexchange pathways. In this article, we report an electronic structure study of $FeGa_2S_4$, $Fe_2Ga_2S_5$, and $NiGa_2S_4$ using photoemission spectroscopy experiments, configuration-interaction calculations on cluster models, and unrestricted Hartree-Fock (HF) calculations on triangular lattice models. The cluster-model analysis of Fe $2p$ core-level spectra shows that the ground states of $FeGa_2S_4$ and $Fe_2Ga_2S_5$ are dominated by the d^6 configuration and that the superexchange interactions between the second- and third-neighbor sites are less important. On the basis of the electronic structure, the fundamental and microscopic interactions on the FeS_2 and NiS_2 triangular lattices are analyzed.

II. EXPERIMENTS

Single crystals of $FeGa_2S_4$, $Fe_2Ga_2S_5$, and $NiGa_2S_4$ were grown by chemical vapor transport as described previously.[14]

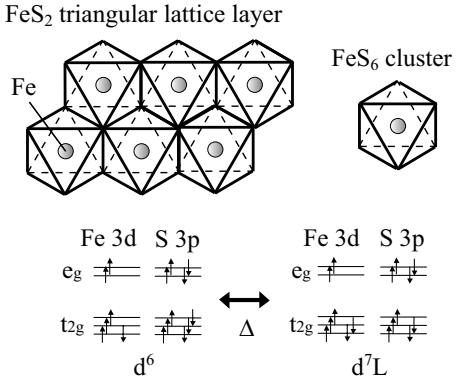

FIG. 1. Schematic drawing for the Fe^{2+} ($S=2$) triangular lattice layer and the electronic configuration of the FeS_6 cluster model used to analyze the photoemission spectra in the same model about the NiS_6 cluster in Ref. 7. The charge-transfer energy Δ is given by the excitation energy from d^6 to d^7L. L denotes a hole in the S $3p$ molecular orbitals.

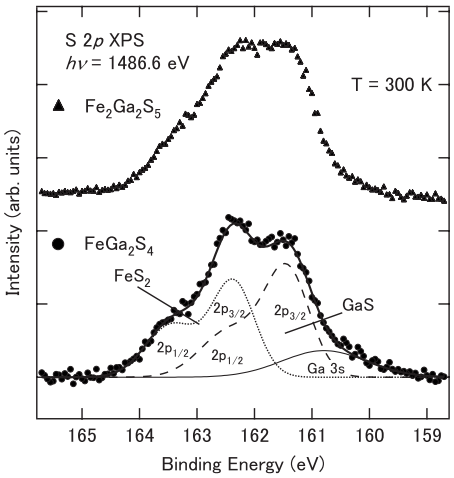

FIG. 2. S $2p$ core-level photoemission spectra of $FeGa_2S_4$ and $Fe_2Ga_2S_5$. The spectra of $FeGa_2S_4$ are decomposed into five Gaussians: the Ga $3s$ component (thin solid curve), the $2p_{3/2}$ and $2p_{1/2}$ components of the GaS layer (dashed curve), and those of the FeS_2 layer (dotted curve). The fitted results are shown by the thick solid curves.

The x-ray photoemission spectroscopy (XPS) were performed using a JPS 9200 spectrometer equipped with a monochromatized Al $K\alpha$ x-ray source ($h\nu$=1486.6 eV). The total-energy resolution was ~0.6 eV and the pressure of the spectrometer was $\sim 1\times 10^{-7}$ Pa during the measurement. The ultraviolet-ray photoemission spectroscopy (UPS) were performed using a SCIENTA SES-100 spectrometer equipped with a He I discharge lamp ($h\nu$=21.2 eV). The total-energy resolution was ~30 meV and the pressure of the spectrometer was $\sim 6\times 10^{-7}$ Pa. The single crystals were cleaved *in situ* in order to obtain clean surfaces. All photoemission data were collected within 48 h after cleaving.

III. RESULTS AND DISCUSSION

A. Photoemission spectroscopy and cluster-model analysis

The S $2p$ core-level photoemission spectra of $FeGa_2S_4$ and $Fe_2Ga_2S_5$ are given in Fig. 2. In the similar way of the previous study of $NiGa_2S_4$,[7] the S $2p$ and Ga $3s$ spectra of $FeGa_2S_4$ are decomposed into five components: the Ga $3s$ component, the S $2p_{3/2}$ and S $2p_{1/2}$ components of the GaS layer, and those of the FeS_2 layer. The magnitude of the energy difference of ~0.9 eV between FeS_2 and GaS is rather small compared to that in the case of $NiGa_2S_4$ (~1.2 eV). On the other hand, the spectra of $Fe_2Ga_2S_5$ cannot be decomposed using five Gaussian components probably because the Fe_2S_3 bilayer has different S sites.

The Fe $2p_{3/2}$ core-level spectra of $FeGa_2S_4$ and $Fe_2Ga_2S_5$ are shown in Fig. 3. The Fe $2p_{3/2}$ spectra of $FeGa_2S_4$ and $Fe_2Ga_2S_5$ consist of two structures: the main peak at ~709 eV and the satellite structures at ~714 eV. In order to extract the electronic structure parameters such as the S $3p$ to Fe $3d$ charge-transfer energy Δ, the Coulomb interaction between the Fe $3d$ electrons U, and the transfer integrals between the S $3p$ and Fe $3d$ orbitals ($pd\sigma$), we have performed configuration-interaction calculations using the octahedral FeS_6 cluster model as the same method about $NiGa_2S_4$ in Ref. 7 (see Fig. 1). The calculated line spectra are broadened and compared with the experimental results in Fig. 3. The Fe $2p_{3/2}$ spectra of $FeGa_2S_4$ and $Fe_2Ga_2S_5$ are reproduced by the calculation using Δ=2.5 eV, U=4.5 eV, and ($pd\sigma$)=−1.1 eV for $FeGa_2S_4$, and

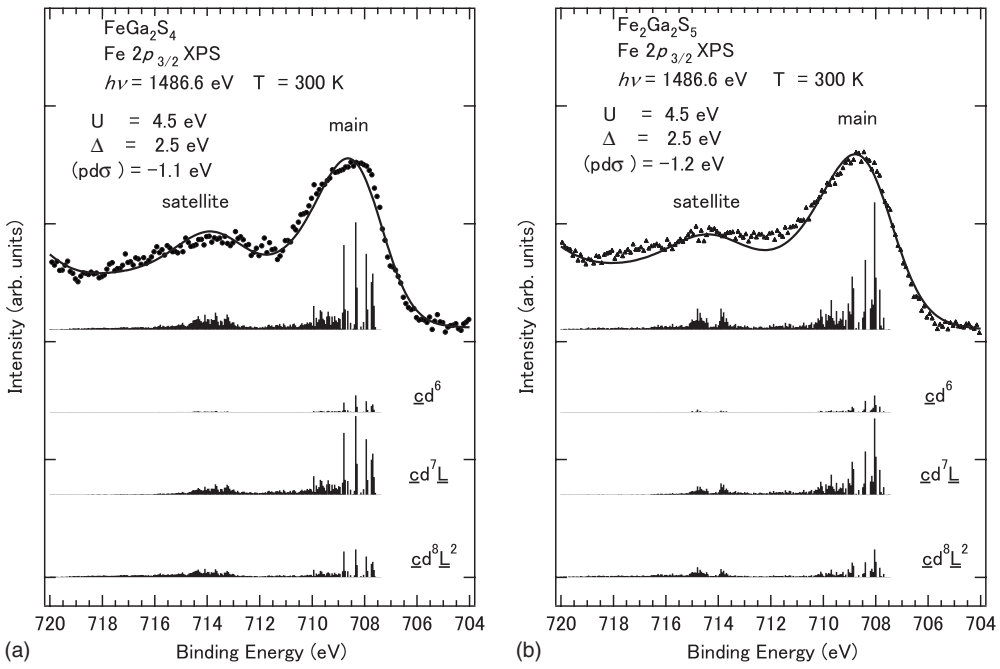

FIG. 3. Fe $2p_{3/2}$ core-level photoemission spectra of (a) $FeGa_2S_4$ and (b) $Fe_2Ga_2S_5$. The calculated line spectra are broadened (solid curve) and are compared with the experimental results. In the lower panel, the line spectrum of Fe $2p$ is decomposed into the cd^6, cd^7L, and cd^8L^2 components.

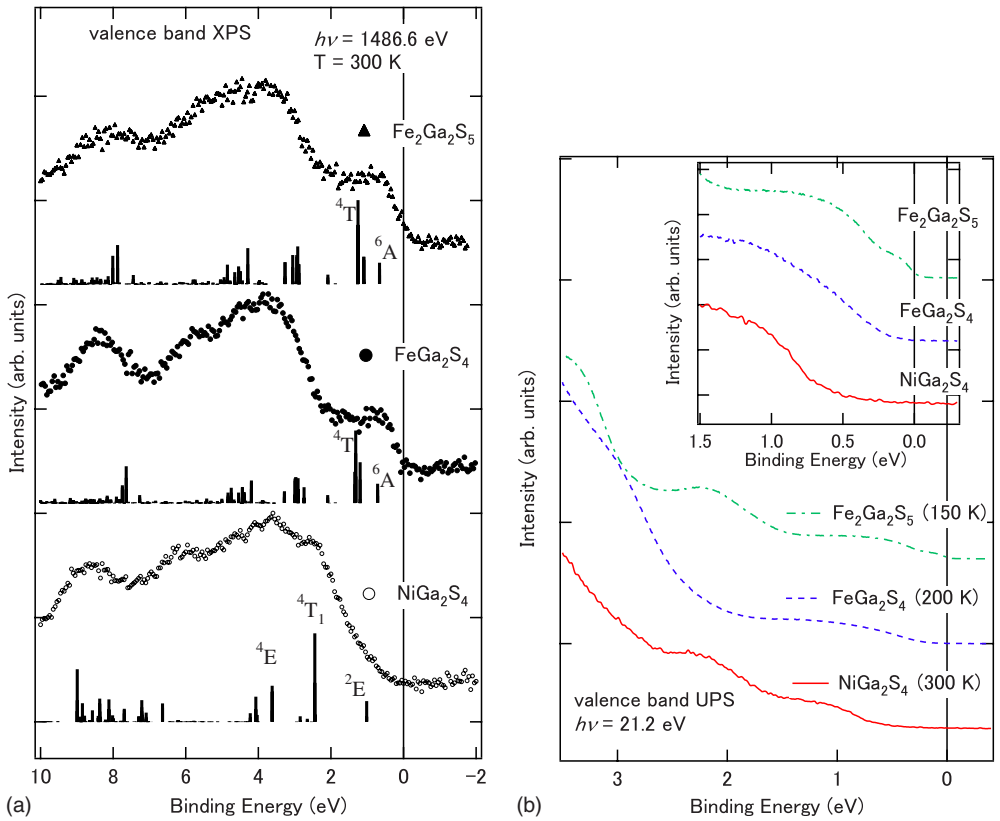

FIG. 4. (Color online) Valence-band (a) XPS and (b) UPS of $FeGa_2S_4Fe_2Ga_2S_5$, and $NiGa_2S_4$. The line spectra in (a) are obtained by the FeS_6 and NiS_6 cluster-model calculations.

Δ=2.5 eV, U=4.5 eV, and $(pd\sigma)$=−1.2 eV for $Fe_2Ga_2S_5$, respectively. The charge-transfer energies of $FeGa_2S_4$ and $Fe_2Ga_2S_5$ are positive, while these are rather small compared to that of other Fe calcogenides.[15] The ground state is given by

$$\Psi_g = \alpha|d^6\rangle + \beta|d^7L\rangle + \gamma|d^8L^2\rangle, \quad (1)$$

The final states are given by the linear combinations of cd^6, cd^7L, and cd^8L^2 configurations, with α^2=0.68, β^2=0.29, and γ^2=0.03 for $FeGa_2S_4$, and α^2=0.66, β^2=0.31, and γ^2=0.03 for $Fe_2Ga_2S_5$. The ground states of $FeGa_2S_4$ and $Fe_2Ga_2S_5$ are dominated by the d^6 configurations and have less S 3p hole characters. This is in striking contrast to the case of the $NiGa_2S_4$. The spectra of Ni $2p_{3/2}$ spectrum of $NiGa_2S_4$ is well reproduced by the calculation with Δ=−1.0 eV, U =5.0 eV, and $(pd\sigma)$=−1.0 eV.[7] The values of α^2, β^2, and γ^2 for $NiGa_2S_4$ are 0.25, 0.60, and 0.15, respectively, and the ground state is dominated by the d^9L configuration. The increase in charge-transfer energy from $NiGa_2S_4$ to $FeGa_2S_4$ is consistent with the chemical trend of charge-transfer energy reported for $Zn_{1-x}Ni_xS$ and $Zn_{1-x}Fe_xS$.[16] The transition-metal 3d level is shifted upwards in going from Ni to Fe as supported by the *ab-initio* calculation.[17] However, the charge-transfer energies of $NiGa_2S_4$ and $FeGa_2S_4$ are by 2.0 and 0.5 eV smaller than those of $Zn_{1-x}Ni_xS$ and $Zn_{1-x}Fe_xS$, respectively, due to the lattice effect.

In Fig. 4, the valence-band XPS and UPS of $FeGa_2S_4$, $Fe_2Ga_2S_5$, and $NiGa_2S_4$ are plotted. The line spectra in Fig. 4(a) are obtained by the FeS_6 and NiS_6 cluster-model calculations for $FeGa_2S_4$, $Fe_2Ga_2S_5$, and $NiGa_2S_4$ with the parameters obtained from the Fe and Ni 2p spectra.[7] In the spectra of $FeGa_2S_4$ and $Fe_2Ga_2S_5$, the first ionization state has the symmetry of $^6A_{1g}$ and the second and third ionization states with $^4T_{1g}$ and $^4T_{2g}$ symmetries are almost degenerate as like FeS.[18] The excitation from the $^5T_{2g}$ ground state to the $^6A_{1g}$ final state mainly consists of removal of a t_{2g} electron. The magnitude of the band gap estimated from the resistivity measurements decreases from $NiGa_2S_4$ (0.28 eV) to $FeGa_2S_4$ (0.11 eV) to $Fe_2Ga_2S_5$ (0.005 eV), while the leading edge of the valence-band spectra is located at ~0.3 eV, 0.1 eV, and 0 eV below E_F for $NiGa_2S_4$, $FeGa_2S_4$, and $Fe_2Ga_2S_5$, respectively [see the inset of Fig. 4(b)]. These values obtained from the photoemission spectra are close to the magnitudes of the band gap estimated from the resistivity, indicating that the Fermi level is located at the top of the band gap in $NiGa_2S_4$, $FeGa_2S_4$, and $Fe_2Ga_2S_5$.[19]

The UPS spectra show additional low-energy structures that are not detected in the XPS spectra. This is probably due to the energy resolution effect and the final-state effect. The energy resolution of the XPS data is about 600 meV while that of the UPS data is about 30 meV. In addition, since the less final states are available in the UPS process than those in the XPS process, the intensity of the Ni 3d bands can be enhanced in a specific region of the momentum space in the UPS spectra. Therefore, the Ni 3d structure can be relatively

sharp in the UPS spectra although the spectra are angle integrated.

In the Ni $2p$ core-level XPS, a Ni $2p$ core hole is created at a Ni site. Therefore, the cluster-model analysis considering a Ni site is valid to analyze the Ni $2p$ core-level XPS. In contrast, the exchange interaction is evaluated using the cell-perturbation method, in which neighboring two Ni sites are considered, and the unrestricted Hartree-Fock method, in which the lattice effect is included. In the three methods, the Coulomb interaction U between the Ni $3d$ electrons is included while the Coulomb interaction U_p between the S $3p$ holes is neglected. In case of $NiGa_2S_4$ with Ni-S-Ni bond angle of 90 degrees, since the Ni $3d$ electron cannot be transferred to the nearest-neighbor site, the antiferromagnetic J_1 term due to U is very weak. Instead, the ferromagnetic J_1 term due to U_p that is not included in the present models becomes dominant. In contrast, the antiferromagnetic J_3 term due to U is much larger than the ferromagnetic J_1 term, and is properly explained by the present model. In $FeGa_2S_4$, since the Fe $3d$ electron can be transferred to the nearest-neighbor site, the J_1 term is dominated by the antiferromagnetic one due to U that is properly included in the present methods.

The Fe $3d$ t_{2g} orbitals of $FeGa_2S_4$ are not fully occupied and the charge-transfer energy is positive ($\Delta=2.5$ eV), while the Ni $3d$ t_{2g} orbitals of $NiGa_2S_4$ are fully occupied and the charge-transfer energy is negative ($\Delta=-1.0$ eV). Therefore, the exchange pathways in $FeGa_2S_4$ (Fe^{2+}, $S=2$) is much different from those in $NiGa_2S_4$ (Ni^{2+}, $S=1$).[7] With the positive Δ and $\beta^2=0.3$, the S $3p$ hole character is relatively weak in the case of $FeGa_2S_4$. As a result, the long superexchange pathways via S $3p$ holes may be negligible in $FeGa_2S_4$. Instead, $FeGa_2S_4$ has an orbital degree of freedom in the t_{2g} states and a slight trigonal distortion of FeS_6 octahedra. In the FeS_6 cluster, the ground state is given by $\Psi_g(^5T_{2g}) = \alpha|d^6(^5T_{2g})\rangle + \beta|d^7L(^5T_{2g})\rangle + \gamma|d^8L^2(^5T_{2g})\rangle$, and the transfer integrals between the neighboring $|d^6(^5T_{2g})\rangle$ states [or $|d^7L(^5T_{2g})\rangle$ states] are given by $\frac{3}{4}(dd\sigma)$ [thick solid line in Fig. 5(a)], which enhance the superexchange interaction between the nearest neighboring sites. The details of the orbital filling and the exchange interaction by the unrestricted HF analysis are given in Sec. III B.

B. Model Hartree-Fock calculation of FeS_2 and NiS_2 triangular lattices

We have examined the electronic structures and exchange interactions of FeS_2 and NiS_2 triangular lattice in $FeGa_2S_4$ and $NiGa_2S_4$ by using the unrestricted HF calculation. The multiband d-p model with $3d$ transition-metal sites are used, in which full degeneracy of the $3d$ orbitals and the ligand $3p$ orbitals are taken into account.[20] The Hamiltonian is given by

$$H = H_p + H_d + H_{pd}, \tag{2}$$

$$H_p = \sum_{\mathbf{k},l,\sigma} \epsilon_k^p p_{\mathbf{k},l\sigma}^+ p_{\mathbf{k},l\sigma} + \sum_{\mathbf{k},l>l',\sigma} V_{\mathbf{k},ll'}^{pp} p_{\mathbf{k},l\sigma}^+ p_{\mathbf{k},l'\sigma} + \text{H.c.}, \tag{3}$$

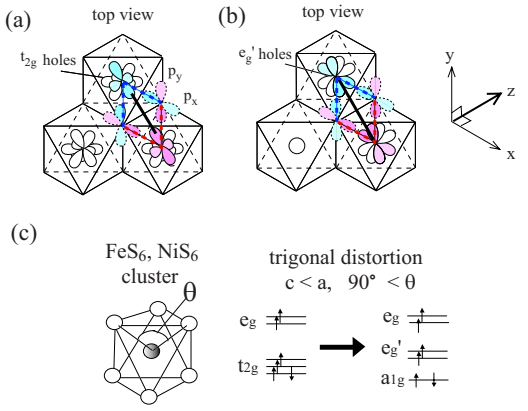

FIG. 5. (Color online) Top views for exchange pathways between the nearest-neighbor clusters in the FeS_2 layer of (a) undistorted case and (b) distorted case ($c<a$). The exchange paths are given by the Fe $3d$-$3d$ direct transfer and Fe $3d$-S $3p$ transfer as indicated by the thick solid line and dashed lines, respectively. (c) Schematic picture of the trigonal distortion of the FeS_6 and NiS_6 clusters and the energy splitting of the Fe^{2+} (d^6) site. θ denotes the S-Fe-S (or S-Ni-S) bond angle.

$$\begin{aligned} H_d = {} & \epsilon_d^0 \sum_{i,m,\sigma} d_{i,m\sigma}^+ d_{i,m\sigma} + u \sum_{i,m} d_{i,m\uparrow}^+ d_{i,m\uparrow} d_{i,m\downarrow}^+ d_{i,m\downarrow} \\ & + u' \sum_{i,m\neq m'} d_{i,m\uparrow}^+ d_{i,m\uparrow} d_{i,m'\downarrow}^+ d_{i,m'\downarrow} \\ & + (u'-j') \sum_{i,m>m',\sigma} d_{i,m\sigma}^+ d_{i,m\sigma} d_{i,m'\sigma}^+ d_{i,m'\sigma} \\ & + j' \sum_{i,m\neq m'} d_{i,m\uparrow}^+ d_{i,m'\uparrow} d_{i,m\downarrow}^+ d_{i,m'\downarrow} \\ & + j \sum_{i,m\neq m'} d_{i,m\uparrow}^+ d_{i,m'\uparrow} d_{i,m'\downarrow}^+ d_{i,m\downarrow}, \end{aligned} \tag{4}$$

$$H_{pd} = \sum_{\mathbf{k},l,m,\sigma} V_{\mathbf{k},lm}^{pd} d_{\mathbf{k},m\sigma}^+ p_{k,l\sigma} + \text{H.c.} \tag{5}$$

where $d_{i,m\sigma}^+$ are creation operators for the $3d$ electrons at site i. $d_{\mathbf{k},m\sigma}^+$ and $p_{\mathbf{k},l\sigma}^+$ are creation operators for Bloch electrons with wave vector $\mathbf{k}$ which are constructed from the mth component of the $3d$ orbitals and from the lth component of the $3p$ orbitals, respectively. The intra-atomic Coulomb interaction between the $3d$ electrons is expressed using Kanamori parameters, u, u', j, and j'.[21] The transfer integrals between the $3d$ and $3p$ orbitals $V_{k,lm}^{pd}$ are given in terms of Slater-Koster parameters $(pd\sigma)$ and $(pd\pi)$. The transfer integrals between the $3p$ orbitals $V_{k,ll'}^{pp}$ are expressed by $(pp\sigma)$ and $(pp\pi)$. Here, the ratios $(pd\sigma)/(pd\pi)$ and $(pp\sigma)/(pp\pi)$, etc. are fixed to Harrison's ratio.[22] In the present calculation, Kanamori parameter $u(=U+20/9j)$, charge-transfer energy Δ, and transfer integrals $(pd\sigma)$ and $(pd\pi)$ are obtained from the Fe $2p$ and Ni $2p$ spectra. Kanamori parameters j and j' are fixed at $j=j'=0.80$ eV for Fe^{2+} and $j=j'=0.88$ eV for Ni^{2+}.[20] $(pp\sigma)$ and $(pp\pi)$ are fixed at 0.60 and -0.15 eV, respectively. Other parameters such as $(dd\sigma)$, $(dd\pi)$, etc. are taken from Ref. [24] and scaled to the bond lengths using

TABLE I. Parameter sets for $FeGa_2S_4$ and $NiGa_2S_4$.

	θ (deg)	U (eV)	Δ (eV)	$(dd\sigma)$ (eV)	$(pd\sigma)$ (eV)
$FeGa_2S_4$	96	4.5	2.5	−0.07	−1.1
$NiGa_2S_4$	97	5.0	−1.0	−0.05	−1.0

Harrison's law. The trigonal distortion of the octahedral cluster[23,24] is also included in the calculation [see Fig. 5(c)]. Here θ denotes the S-Fe-S (or S-Ni-S) bond angle. When the lattice is distorted, the transfer integrals are also scaled using Harrison's law. The representative parameters are listed in Table I. The 3×3, 4×4, and 6×6 unit cells of the FeS_2 or NiS_2 triangular lattice are considered to evaluate various spin structures (Fig. 6).

First, let us discuss the FeS_2 case. Figure 7 is the calculated HF energy for FeS_2 triangular lattice for various spin structures at θ=90° and θ=96°. Spin structures labeled as (I)–(VII) are displayed in Fig. 6. The lowest-energy state of FeS_2 triangular lattice with θ=90° is structure (VI) of 180° 1×2 type, although the lowest-energy state of a simple antiferromagnetic triangular lattice is supposed to be structure (II) of 120° $\sqrt{3}\times\sqrt{3}$ in the mean-field regime. Structure (VI) is stabilized when the second-nearest-neighbor interaction is embedded in Ref. 25. When the lattice distortion (θ=96°) is taken into account, structure (II) decreases in energy and becomes the lowest-energy state. The energy difference between structures (II) and (VI) is very small and the true ground state cannot be determined in the present mean-field calculation. Here, we have only discussed the tendency of the exchange paths. As a slight trigonal distortion of FeS_6 octahedra, the t_{2g} states split into a lower a_{1g} state and two higher e_g' states and the holes mainly occupy the $e_{g\downarrow}'$ states [Fig. 5(c)]. Figure 8 is the calculated density of states for the lowest-energy state compared with the XPS data of $FeGa_2S_4$. The top of the valence band is made up from the $a_{1g\downarrow}$ state and the calculated band gap is ~3.1 eV.

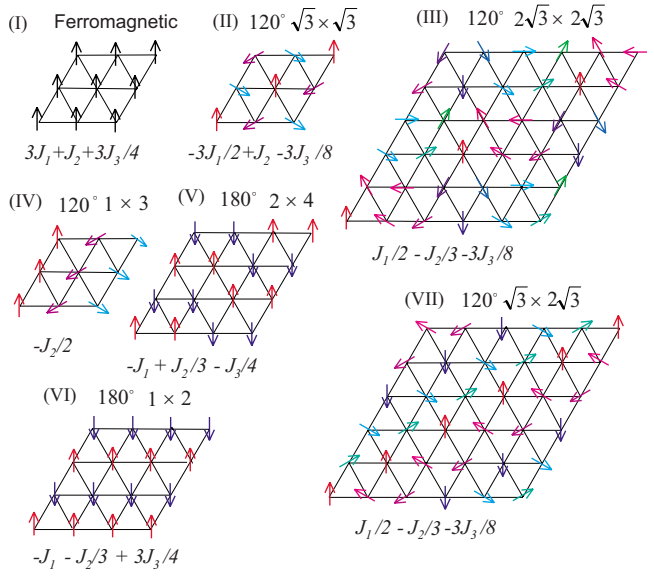

FIG. 6. (Color online) Various spin structures for the calculation on the FeS_2 and NiS_2 triangular lattices. All spin axes are assumed to lie in the triangular plane.

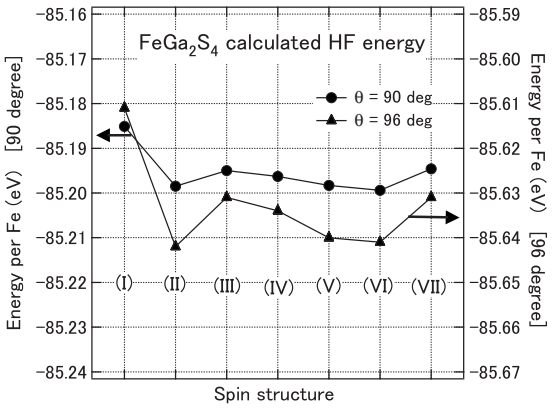

FIG. 7. Calculated Hartree-Fock energy of $FeGa_2S_4$ for the various spin structures. (I)–(VII) denote the spin structures in Fig. 6.

The calculated Hartree-Fock energies E_I-E_{VII} with spin structures (I)–(VII) can be used to evaluate the strength of exchange interactions J_1, J_2, and J_3 in the Heisenberg model. The energies can be expressed using the exchange interactions as follows:

$$E_I = \left(3J_1 + J_2 + \frac{3}{4}J_3\right)S^2,$$

$$E_{II} = \left(-\frac{3}{2}J_1 + J_2 - \frac{3}{8}J_3\right)S^2,$$

$$E_{III} = \left(\frac{1}{2}J_1 - \frac{1}{3}J_2 - \frac{3}{8}J_3\right)S^2,$$

$$E_{IV} = \left(-\frac{1}{2}J_2\right)S^2,$$

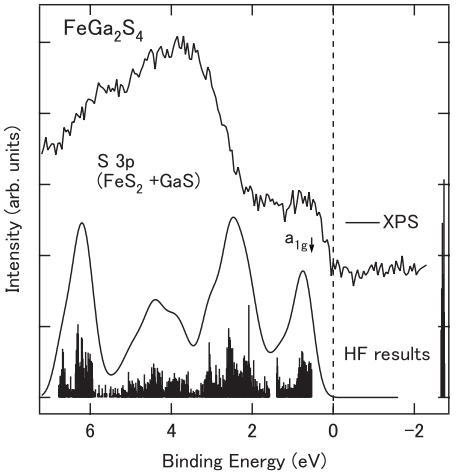

FIG. 8. Calculated Hartree-Fock density of states for $FeGa_2S_4$ [θ=96°, structure (II)] compared with the XPS data. The contribution from GaS layer (with S 3p character) is also located around 4–10 eV for the XPS data.

TABLE II. Exchange interactions J_1, J_2, and J_3 for $FeGa_2S_4$.

	J_1 (meV)	J_2 (meV)	J_3 (meV)
$\theta=90°$	$-0.7^{+0.3}_{-0.1}$	$-0.3^{+0.1}_{-1.0}$	$-0.2^{+2.1}_{-0.4}$
$\theta=96°$	$-1.8^{+0.2}_{-0.2}$	$-0.3^{+0.2}_{-0.2}$	$-0.2^{+0.7}_{-0.7}$

$$E_{\mathrm{V}} = \left(-J_1 - \frac{1}{3}J_2 + \frac{3}{4}J_3\right)S^2,$$

$$E_{\mathrm{VI}} = \left(-J_1 + \frac{1}{3}J_2 - \frac{1}{4}J_3\right)S^2,$$

$$\left[E_{\mathrm{VII}} = \left(\frac{1}{2}J_1 - \frac{1}{3}J_2 - \frac{3}{8}J_3\right)S^2\right]. \quad (6)$$

Here, structure (VII) is omitted because the energy is almost equal to (III). J_1, J_2, and J_3 for $FeGa_2S_4$ are estimated as listed in Table II using the least square method. The interaction between the first-neighbor sites J_1 is smaller than that between the second-neighbor sites J_2 and third-neighbor sites J_3. At $\theta=90°$, J_2 is small enough against J_1 to stabilize the structure of (VI). On the other hand, in the distorted lattice ($\theta=96°$), both of the e'_g-e'_g direct hopping and the e'_g-S $3p$-type transfer are enhanced due to e_g-t_{2g} mixing and cause the strong antiferromagnetic interaction between the first-neighbor sites [Fig. 5(b)]. Thus, J_1 becomes much smaller compared to the long-range interactions J_2 and J_3. At both cases of $\theta=90°$ and $\theta=96°$, the third-neighbor interaction J_3 is negligibly weak in $FeGa_2S_4$.

In case of $NiGa_2S_4$, the lowest-energy state at the HF calculation also has structure (II) of 120° $\sqrt{3}\times\sqrt{3}$ type (Fig. 9). However the observed spin structure in the neutron experiments for $NiGa_2S_4$ (Ref. 4) is a noncollinear structure in which the angle between the first-neighbor spins are ~57° (~half of 120°) and near to type (III) or (VII) spin structures. This is partly due to ferromagnetic interactions between the first-neighbor sites competing with antiferromagnetic interactions between the third-neighbor sites. As discussed in the previous work,[7] the ferromagnetic component in J_1 comes

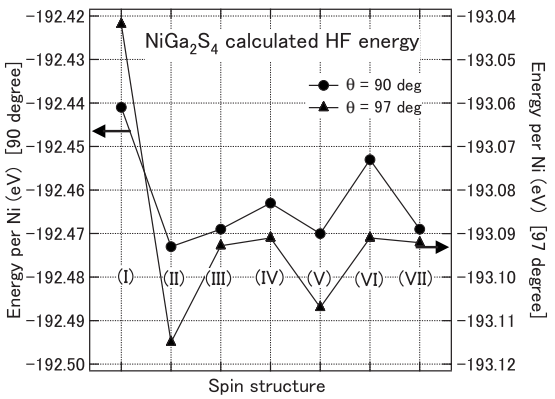

FIG. 9. Calculated Hartree-Fock energy of $NiGa_2S_4$ for the various spin structures. (I)–(VII) denote the spin structures in Fig. 6.

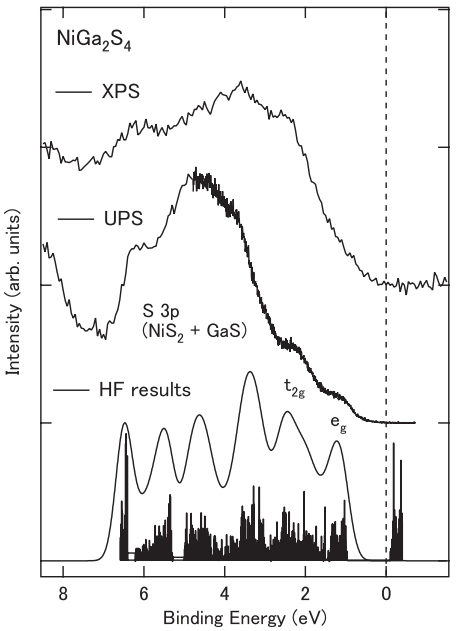

FIG. 10. Calculated Hartree-Fock density of states for $NiGa_2S_4$ [$\theta=97°$, structure (II)] compared with XPS and UPS data. The contribution from GaS layer (with S $3p$ character) is also located around 4–10 eV for the photoemission data.

from the Hund coupling between the S $3p$ holes at the same S sites (J_p). However, this effect is dismissed in the p-d Hamiltonian of the present calculation. Even in this regime, the calculated density of states for NiS_2 well reproduces the XPS and UPS spectra and the band gap is ~1.0 eV (Fig. 10). The e_g and t_{2g} bands are assigned to the structures around ~1.5 eV and ~2.5 eV, respectively.

The magnetic interactions J_1, J_2, and J_3 in NiS_2 layer are also evaluated and the results are shown in Table III. At $\theta=90°$, the interaction between the third-neighbor sites J_3 is significantly smaller than that between the first-neighbor sites J_1 and second-neighbor sites J_2, consistent with the results of the cell perturbation. On the other hand, J_1 at $\theta=97°$ is estimated to be ~−12 meV, although J_1 is ferromagnetic in the magnetic experiments.[4,5] Similar to $FeGa_2S_4$, the lattice distortion enhances the e_g-S $3p$-type hopping. Thus the antiferromagnetic interaction between the first-neighbor sites is overestimated in the condition without J_p. Even in this condition, the third-neighbor interaction J_3 is retained at small value (~−17.9 meV) in case of $NiGa_2S_4$, contrary to the case of $FeGa_2S_4$.

In order to clarify the difference of the exchange interaction of the triangular lattice between $FeGa_2S_4$ and $NiGa_2S_4$,

TABLE III. Exchange interactions J_1, J_2, and J_3 for $NiGa_2S_4$ calculated from the HF calculation and those estimated using a cell-perturbation approach in the previous study (Ref. 7).

	J_1 (meV)	J_2 (meV)	J_3 (meV)
$\theta=90°$	$-2.3^{+0.4}_{-0.6}$	$-0.5^{+0.5}_{-1.0}$	$-18.0^{+0.9}_{-0.8}$
$\theta=97°$	$-12.0^{+1.8}_{-1.2}$	$-0.3^{+0.6}_{-0.4}$	$-17.9^{+0.4}_{-1.6}$
Previous study	−1	−1	−14

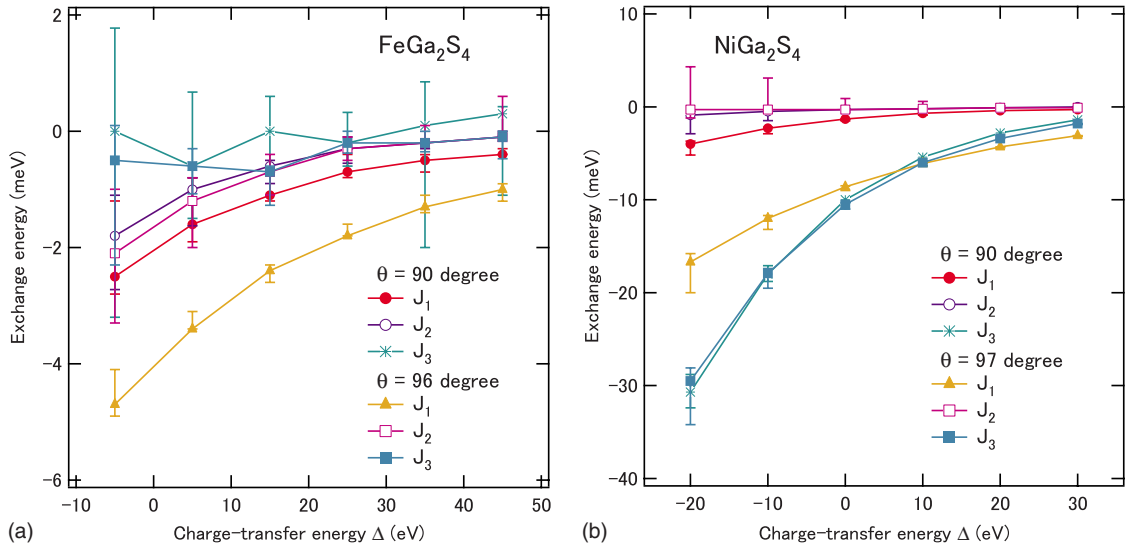

FIG. 11. (Color online) Charge-transfer energy Δ dependence of the exchange interactions J_1, J_2, and J_3 for (a) $FeGa_2S_4$ and (b) $NiGa_2S_4$ estimated from the HF calculations.

Δ dependence of the exchanges J_1, J_2, and J_3 is plotted in Fig. 11. J_3 of $NiGa_2S_4$ becomes smaller for smaller Δ. On the other hand, the magnitude of J_3 for $FeGa_2S_4$ has no clear dependence on Δ, corresponding to the difference of the electronic configuration.

Our HF results on $NiGa_2S_4$ are basically consistent with the results of the local-density approximation (LDA) by Mazin.[26] The LDA+U result with U=6 eV has provided the strong third-neighbor interaction and the substantial amount of S 3p holes, similar to the HF result of this study. This indicates that the contribution of the S-S hopping is also included in the LDA+U calculation as well as in the HF calculation on the triangular lattice. Moreover, the LDA+U calculation and the present HF calculation commonly predict that J_1 is antiferromagnetic and that the magnitude of J_1 is comparable to that of J_3, insufficient to explain the observed magnetic structure. As pointed out in our cell-perturbation calculation,[7] the Hund coupling between the two S 3p holes should be considered to have ferromagnetic J_1. In this sense, the cell perturbation on the S-S hopping term is still useful to explain the observed magnetic structure of $NiGa_2S_4$. Reference 26 has also argued about Na_xCoO_2. However, since the charge-transfer energy is also very small,[27] the O-O hopping term is expected to be important for Na_xCoO_2. Therefore, the cell perturbation on the O-O hopping term would be useful for Na_xCoO_2. It would be interesting to systematically study the exchange interactions in Na_xCoO_2 by means of unrestricted HF and cell-perturbation calculations.

IV. SUMMARY

The electronic structures of $FeGa_2S_4$, $Fe_2Ga_2S_5$, and $NiGa_2S_4$ with the FeS_2 and NiS_2 triangular lattices are investigated using photoemission experiments and model HF calculations. The band gap becomes smaller from $NiGa_2S_4$ to $FeGa_2S_4$, to $Fe_2Ga_2S_5$, consistent with the resistivities. The Fe 2p data and the cluster-model analysis indicate that the d^6 states are dominant in $FeGa_2S_4$ and $Fe_2Ga_2S_5$. The charge-transfer energies are positive and the S 3p hole character is weak. The e_g'-e_g' direct hopping and e_g'-S 3p-e_g' superexchange give the superexchange interaction between the first-nearest-neighbor sites in the $FeGa_2S_4$. The density of states of FeS_2 and NiS_2 layers calculated using the unrestricted HF calculation well reproduces the experimental spectra for $FeGa_2S_4$ and $NiGa_2S_4$. The spin structure and the exchange interaction are also analyzed based on the HF results.

ACKNOWLEDGMENTS

The authors would like to thank H. Wadati, A. Damascelli, D. Fournier, and G. Levy for valuable discussions. The authors further wish to thank Y. Maeno for his support of this study. This work was supported by a Grant-In-Aid for Scientific Research (Grant No. 19340092) from the Ministy of Education, Culture, Sports, Science and Technology of Japan. K.T. acknowledges support from the Japan Society for the Promotion of Science for Young Scientists. This work was supported in part by Grant-in-Aids for Scientific Research (Grant Nos. 17071003, 18684020, and 19052003) from MEXT, Japan.

[1] M. F. Collins and O. A. Petrenko, Can. J. Phys. **75**, 605 (1997).
[2] R. Moessner and S. L. Sondhi, Phys. Rev. Lett. **86**, 1881 (2001).
[3] Y. Shimizu, K. Miyagawa, K. Kanoda, M. Maesato, and G. Saito, Phys. Rev. Lett. **91**, 107001 (2003).
[4] S. Nakatsuji, Y. Nambu, H. Tonomura, O. Sakai, S. Jonas, C. Broholm, H. Tsunetsugu, Y. Qiu, and Y. Maeno, Science **309**, 1697 (2005).
[5] H. Takeya, K. Ishida, K. Kitagawa, Y. Ihara, K. Onuma, Y. Maeno, Y. Nambu, S. Nakatsuji, D. E. MacLaughlin, A. Koda, and R. Kadono, Phys. Rev. B **77**, 054429 (2008).
[6] S. Nakatsuji, H. Tonomura, K. Onuma, Y. Nambu, O. Sakai, Y. Maeno, R. T. Macaluso, and J.-Y. Chan, Phys. Rev. Lett. **99**, 157203 (2007).
[7] K. Takubo, T. Mizokawa, J. Y. Son, T. Nambu, S. Nakatsuji, and Y. Maeno, Phys. Rev. Lett. **99**, 037203 (2007).
[8] H. Tsunetsugu and M. Arikawa, J. Phys. Soc. Jpn. **75**, 083701 (2006).
[9] S. Fujimoto, Phys. Rev. B **73**, 184401 (2006).
[10] A. Läuchli, F. Mila, and K. Penc, Phys. Rev. Lett. **97**, 087205 (2006).
[11] S. Bhattacharjee, V. B. Shenoy, and T. Senthil, Phys. Rev. B **74**, 092406 (2006).
[12] P. Li, G. M. Zhang, and S. Q. Shen, Phys. Rev. B **75**, 104420 (2007).
[13] H. Kawamura and A. Yamamoto, J. Phys. Soc. Jpn. **76**, 073704 (2007).
[14] Y. Nambu, M. Ichihara, Y. Kiuchi, S. Nakatsuji, and Y. Maeno, J. Cryst. Growth **310**, 1881 (2008).
[15] A. E. Bocquet, T. Mizokawa, T. Saitoh, H. Namatame, and A. Fujimori, Phys. Rev. B **46**, 3771 (1992).
[16] T. Mizokawa and A. Fujimori, Phys. Rev. B **48**, 14150 (1993).
[17] S. Watanabe and H. Kamimura, J. Phys. Soc. Jpn. **56**, 1078 (1987).
[18] K. Shimada, T. Mizokawa, K. Mamiya, T. Saitoh, A. Fujimori, K. Ono, A. Kakizaki, T. Ishii, M. Shirai, and T. Kamimura, Phys. Rev. B **57**, 8845 (1998).
[19] T. Tomita, H. Tonomura, Y. Nambu, Y. Matsumoto, S. Nakatsuji, Y. Maeno, K. Matsubayashi, and Y. Uwatoko, J. Phys. Soc. Jpn. (to be published).
[20] T. Mizokawa and A. Fujimori, Phys. Rev. B **54**, 5368 (1996).
[21] J. Kanamori, Prog. Theor. Phys. **30**, 275 (1963).
[22] W. A. Harrison, *Electronic Structure and the Properties of Solid* (Dover, New York, 1989).
[23] H. D. Lutz, W. Buchmeier, and H. Siwert, Z. Anorg. Allg. Chem. **533**, 118 (1986).
[24] L. Dogguy-Smiri, N.-H. Dung, and M. P. Pardo, Mater. Res. Bull. **15**, 861 (1980).
[25] S. Katsura, T. Ide, and T. Morita, J. Stat. Phys. **42**, 381 (1986).
[26] I. I. Mazin, Phys. Rev. B **76**, 140406(R) (2007).
[27] T. Kroll, A. A. Aligia, and G. A. Sawatzky, Phys. Rev. B **74**, 115124 (2006).